Available online at www.sciencedirect.com
SCIENCE DIRECT®
PERGAMON
International Journal of Heat and Mass Transfer 46 (2003) 4071–4081
International Journal of HEAT and MASS TRANSFER
www.elsevier.com/locate/ijhmt

Momentum transport at a fluid–porous interface

B. Goyeau [a,c,*], D. Lhuillier [b], D. Gobin [a], M.G. Velarde [c]

[a] *Fluides, Automatique et Systèmes Thermiques, FAST, UMR-CNRS 7608, Universités Paris VI et Paris XI Campus Universitaire, Bât. 502, 91405 Orsay Cedex, France*

[b] *Laboratoire de Modélisation Mécanique, LMM, Université Paris VI, UMR CNRS 7607, 4, place Jussieu, Tour 66 Case 162, 75252, Paris Cedex 05, France*

[c] *Instituto Pluridisciplinar, Universidad Complutense de Madrid. Paseo Juan XXIII, n. 1, E-28040 Madrid, Spain*

Received 17 February 2003

Abstract

The momentum balance at the interface between a liquid and a porous substrate is investigated for a configuration with forced flow parallel to the interface. An heterogeneous continuously varying transition layer between the two outer bulk regions is introduced. The stress jump coefficient earlier introduced in the jump interface condition is here derived as an explicit function of the variations of the velocity and effective properties of the transition layer. Agreement is found between our numerical results based on the single-domain approach and the existing ad hoc estimates in the literature. Further advantages of this non-homogeneous analysis are also provided.

1. Introduction

Transport phenomena in structures composed by a porous layer and an adjacent fluid are encountered in a wide range of industrial applications (thermal insulation, filtration processes, dendritic solidification, storage of nuclear waste, drying processes, spreading on porous substrates, ...) or environmental context (geothermal systems, benthic boundary layers, ground-water pollution, ...). The underlying modeling problem lies in the coupling between conservation equations in both regions and thus in the definition of appropriate boundary conditions at the fluid/porous interface. An accurate description of the convective heat or species transfer involved in the above-mentioned processes depends on the relevance of the momentum transport model at the interface. Due to its theoretical and practical interest, this question has been the subject of an intense research activity recently reviewed in the field of transport in porous media [1,2]. The two different approaches generally proposed to deal with this problem will be discussed in the present section.

1.1. The two-domain approach

The first studies concerning flow in a fluid/porous configuration have been devoted to the calculation of the drag force exerted by a fluid on a porous sphere [3–6] while other motivations were related to lubrification of porous-bearings [7,8]. The study by Beavers and Joseph (BJ) provides an experimental and analytical study of fluid flow past a porous material, focusing on the boundary condition at the fluid/porous interface. In order to describe the forced flow in the composite channel (Fig. 1), a Stokes flow is considered in the fluid region while the momentum transport in the homogeneous porous layer is described by Darcy's law. Due to the different order of the corresponding partial differential equations a semi-empirical slip boundary condition is proposed at the interface

$$\left.\frac{\partial u}{\partial y}\right|_{y=0} = \frac{\alpha}{K^{1/2}}\left(u(0) - U(-H)\right) \tag{1}$$

* Corresponding author. Address: Fluides, Automatique et Systèmes Thermiques, FAST, UMR-CNRS 7608, Universités Paris VI et Paris XI Campus Universitaire, Bât. 502, 91405 Orsay Cedex, France. Tel.: +33-1-69-15-80-39; fax: +33-1-69-15-80-60.

E-mail address: goyeau@fast.u-psud.fr (B. Goyeau).

0017-9310/03/$ - see front matter © 2003 Elsevier Ltd. All rights reserved.
doi:10.1016/S0017-9310(03)00241-2

Nomenclature

Da	Darcy number
d_p	pore size diameter, m
d_p^*	dimensionless pore size diameter
h	thickness of the fluid channel, m
H	thickness of the homogeneous porous layer, m
K	permeability, m^2
u	fluid velocity, $m\,s^{-1}$
U	seepage velocity in the porous layer, $m\,s^{-1}$

Greek symbols

α	slip coefficient
β	stress jump coefficient
δ	thickness of the non-homogeneous porous layer, m
δ_T	total porous boundary layer thickness
δ_B	Brinkman boundary layer
ε_f	porosity
η	dimensionless reduced viscosity
Φ	fractional increase in mass flow rate
μ	dynamic fluid viscosity, $kg\,m^{-1}\,s^{-1}$
μ_{eff}	effective dynamic fluid viscosity, $kg\,m^{-1}\,s^{-1}$
ρ	fluid density, $kg\,m^{-3}$
σ	$1/\sqrt{Da}$

Subscripts

f	fluid
H	homogeneous porous medium

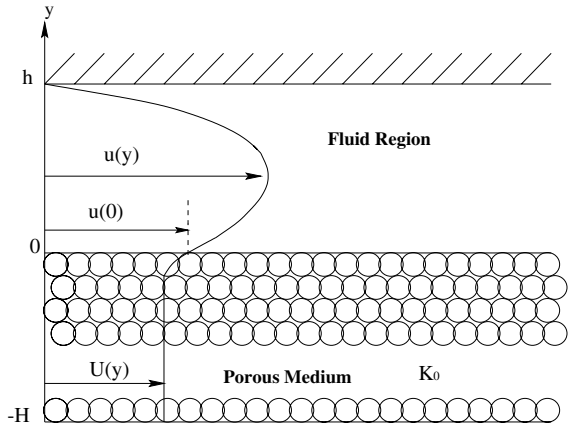

Fig. 1. Poiseuille flow in a fluid/porous channel.

where $u(y)$ is the fluid velocity in the fluid channel, U the seepage velocity, K the permeability of the porous material and α an empirical dimensionless slip coefficient. A theoretical justification of condition (1) is given by Saffman [9] using a statistical approach and a boundary layer approximation, which shows that the "outer" flow is correctly determined by $\mathcal{O}(K^{1/2})$. In this analysis, $u(0)$ is found to be very sensitive to the location of the interface which actually remains unknown [10]. This dependence has been numerically quantified by examining the axial and transverse flows near the surface of two-dimensional periodic porous media [11,12]. Several studies have focused on the determination of the slip parameter α which has been found to be strongly dependent on the local geometry of the interface [13–15] but not on the nature of the fluid [16]. The experimental data provided by [8] are in good agreement with the analytical solutions by adjusting the values of α between 0.1 and 4 depending on the nature of the porous layer (foametal and aloxite specimens). This wide range of α variations clearly shows the importance of the porous structure at the interface even for materials having roughly the same macroscopic average properties in the core [17].

An alternative model has been proposed using the Brinkman equation [18] in the porous layer [19]

$$0 = -\nabla P + \rho_f\,\mathbf{g} - \mu_f \mathbf{K}^{-1}\mathbf{V} + \mu_{eff}\nabla^2\mathbf{V} \tag{2}$$

where μ_{eff} is the effective viscosity and $\mathbf{V}$ is the filtration velocity vector. Since the Stokes and Brinkman equations are of the same order, continuity of both stress and velocity can be satisfied at the interface. In that case, the analytical solution in the bulk fluid is similar to the solution by BJ provided that $\alpha = (\mu_{eff}/\mu_f)^{1/2}$. Eq. (1) then becomes

$$\left.\frac{\partial u}{\partial y}\right|_{y=0} = \sqrt{\frac{\mu_{eff}/\mu_f}{K}}(u(0) - U(-H)) \tag{3}$$

This formulation accounts for momentum transport in the porous layer at a thickness δ estimated to be on the order of $K^{1/2}$. The validity of Brinkman equation has been the subject of extensive and controversial literature [20–29] that we shall not develop in the frame of this paper. Let us only recall two main limitations: first, the Brinkman correction is significant only for high porosity values, second, the effective viscosity, which depends on the structure of the porous material, may strongly differ from the viscosity of the fluid. Although this latter aspect may be important, only a few studies have been devoted to the determination of the effective viscosity over the last 30 years [11,12,21,24,30–36]. Most of them concern sparse porous structures or dilute suspensions for which the reduced viscosity is found to be close to

Einstein's law [37]: $\mu_{\text{eff}}/\mu_{\text{f}} = 1 + 2.5\phi$ where ϕ is the solid volume fraction. Using the statistical approach proposed by Saffman [9], Lundgren [21] examined the relevance of the Brinkman correction for denser beds of spheres and suspensions. According to Saffman, the friction term is not only proportional to the velocity but also depends on its derivative and in that case, the comparison with the Stokes term allows for the determination of the effective viscosity. In moderately dense suspensions, the reduced viscosity is given by $\mu_{\text{eff}}/\mu_{\text{f}} = 1/(1 - 2.5\phi)$ while the evolution for a "dense" bed of spheres shows a surprising non-monotonic behavior with a rapid decrease for $\phi \gtrsim 0.3$. This unexpected behavior is attributed to the interactions between particles that are not correctly described for dense systems. On the contrary, recent numerical calculations for relatively dense systems ($0.2 \leqslant \phi \leqslant 0.5$) show the monotonic behavior of the effective viscosity [35]. The influence of the flow through the Reynolds number also has been analyzed [36,38]. The derivation of a correct law for the effective viscosity is still under investigation [39] and it probably depends on the tortuosity of the medium [40].

Returning to the stress boundary condition, the latest model [41,42] introduces an interfacial jump condition based on the non-local form of the volume averaged Stokes's equation

$$\mu_{\text{f}} \left.\frac{\partial u}{\partial y}\right|_{y=0} - \mu_{\text{eff}} \left.\frac{\partial U}{\partial y}\right|_{y=0} = -\frac{\beta}{\sqrt{K}} u(0) \tag{4}$$

where β is an adjustable parameter which must be experimentally determined. This description assumes that the porous layer is *homogeneous*, and comparing condition (4) to (3), it may be written

$$\left.\frac{\partial u}{\partial y}\right|_{y=0} = \sqrt{\frac{\mu_{\text{eff}}/\mu_{\text{f}}}{K}}(u(0) - U(-H)) - \frac{\beta}{\sqrt{K}} u(0) \tag{5}$$

The analytical solutions of this model are in good agreement with the experimental results of BJ for β on the order of one but unfortunately, no explicit dependence with the geometry of the interface is provided. Actually, condition (4) is an equivalent representation of the spatial variations of the porous structure at the interface. We will see in Section 3 how the stress jump coefficient can be explicitly deduced from an alternative non-homogeneous description of the interface. Such a stress jump condition (4) has been also used when inertia is significant [43] or for a Couette flow in a composite channel [44].

Several numerical studies describe the interfacial flow for fractal porous geometries [45], periodic arrays of spheres [46] or rods [11,12,38,47]. James and Davis [47] use a singularity method to solve the flow field at the interface of a fibrous porous medium. For very large values of the porosity (greater than 0.9) their analysis mainly focuses on the slip velocity for both shear- and pressure-driven flows. In both cases, it is found that the Brinkman model strongly overestimates the flow penetration and the slip velocity.

1.2. The single-domain approach

In this approach, the porous layer is considered as a pseudo-fluid and the composite region is treated as a continuum. The transition from the fluid to the porous medium is achieved through a continuous spatial variation of properties, such as the permeability in the Darcy term of the modified Navier–Stokes equations [48–50]. If the porous layer is assumed to be homogeneous, this equation takes the form

$$\begin{aligned}\varepsilon^{-1}\frac{\partial}{\partial t}(\rho_{\text{f}}\mathbf{V}) + \varepsilon^{-2}\nabla\cdot(\rho_{\text{f}}\mathbf{V}\mathbf{V}) \\ = -\nabla P + \rho_{\text{f}}\mathbf{g} - \mu_{\text{f}}\mathbf{K}^{-1}\mathbf{V} + \mu_{\text{eff}}\nabla^2\mathbf{V}\end{aligned} \tag{6}$$

where ε is the local porosity of the domain. In the liquid channel, $\varepsilon = 1$, $\mu_{\text{eff}} = \mu_{\text{f}}$ and the permeability is infinite, so that the Darcy term is equal to zero and (6) is the Navier–Stokes equation. In the homogeneous porous medium, $\varepsilon = \varepsilon_{\text{f}}$, and the effective viscosity and the permeability values are given by the corresponding relations. Note that for finite values of the permeability, all the terms involving the velocity are formally retained but the Darcy's term is predominant.

Since this formulation avoids the explicit formulation of the boundary conditions at the fluid/porous interface, it has been extensively used in numerical computations dealing with thermal natural convection [50–55] or double diffusive convection [56,57]. A good agreement has been obtained in the comparison with experimental results [49,50,58] using $\mu_{\text{eff}} = \mu_{\text{f}}$ in the calculations.

1.3. Objectives

The above discussion shows that the main features of interfacial momentum transport are rather well understood. However, some fundamental questions concerning the correct formulation are still open and deserve some attention. In the two-domain approach, often presented as more rigorous, the solutions are in agreement with the experimental observations only after adjusting the ad hoc parameters α or β. Those parameters are said to depend on the structural characteristics of the porous interface, but no explicit relation has been provided so far. Also it is still not clear in which situations the continuity of the velocity associated to a stress jump condition (4) gives a better description than the models by [8] or [19]. On the other hand, the single-domain approach remains questionable since the physical representation of momentum conservation in the interfacial region depends on the relevance of the discretization scheme.

The purpose of this study is to tackle to the above questions by means of a thorough quantitative comparison of the single- and the two-domain approaches and by non-homogeneous description of the interface. We first assume that the porous material is *homogeneous* (foametal structures), and we examine the *limitations* of the existing models by comparing the numerical solutions of the single-domain formulation to the analytical and experimental results provided by BJ (Section 2). In Section 3, an *alternative analysis* is proposed to focus on situations where the porous substrate is characterized by *evolving heterogeneities* near the interface, i.e., where there are continuous spatial variations of the effective properties as in aloxite structures. Then, the stress jump coefficient β is expressed as a function of the variations of the velocity and effective properties. Agreement is found between our numerical results based on the single-domain approach and the existing ad hoc estimates in the literature while advantages of the *non-homogeneous* analysis are emphasized. Finally, we conclude that our analysis constitutes an "intermediate" step towards the exact determination of β, which would imply to write a general closure problem at the fluid/porous interface, which still remains a challenge.

2. Single- or two-domain model: a quantitative comparison

The basic configuration considered in this section (Fig. 1) is the fluid/porous composite channel studied by [8]. The saturated porous region is homogeneous and the flow is assumed to be stationary and incompressible. Inertia effects in both regions are neglected. The two-domain model uses the Brinkman equation in the porous layer, and the Stokes one in the fluid. If continuity is satisfied for shear stress and velocity at the fluid/porous interface [19], the dimensionless dynamic boundary conditions of the problem are given by

$$u(1) = 0 \tag{7}$$

$$U(0) = u(0) \tag{8}$$

$$\left.\frac{\partial u}{\partial y}\right|_{y=0} = \alpha^2 \left.\frac{\partial U}{\partial y}\right|_{y=0} \tag{9}$$

$$U(-H^*) = -Da\frac{\mathrm{d}P}{\mathrm{d}x} \tag{10}$$

where $Da = K_0/h^2$ is the Darcy number, K_0 being the permeability of the porous layer, H^* its dimensionless thickness ($H^* = H/h$) and $\alpha^2 = \mu_{\mathrm{eff}}/\mu_{\mathrm{f}}$ the reduced viscosity. The analytical solution of the two-domain model is easily determined

$$u(y) = U(-H^*)\left\{\frac{\sigma(\sigma+2\alpha)}{2(1+\sigma\alpha)} + \frac{\alpha(\sigma^2-2)}{2(1+\sigma\alpha)}(y\sigma) - \frac{1}{2}(y\sigma)^2\right\} \quad 0 \leqslant y \leqslant 1 \tag{11}$$

$$U(y) = U(-H^*)\left\{1 + \frac{\sigma^2-2}{2(1+\sigma\alpha)}\exp\left(\frac{1}{\alpha}y\sigma\right)\right\} \quad -H^* \leqslant y \leqslant 0 \tag{12}$$

where $\sigma = 1/\sqrt{Da}$, following the BJ nomenclature. According to the above assumptions, the momentum transport equation (6) for the single-domain model also reduces to

$$0 = -\frac{\mathrm{d}P}{\mathrm{d}x} - \frac{1}{Da}U + \alpha^2\frac{\mathrm{d}^2U}{\mathrm{d}y^2} \quad -H^* \leqslant y \leqslant 0 \tag{13}$$

in the whole channel, where the Da and α values depend on the region. The numerical approximation of this differential equation is based on a standard finite volume procedure [59]. The numerical results presented hereafter are obtained using regular or irregular node distribution in the y-direction depending on the homogeneous (Section 2) or heterogeneous (Section 3) character of the porous layer. The validation of the numerical model has been performed using the exact analytical solution of the Poiseuille flow when the porous wall is impermeable ($Da \to 0$). The comparison with the experimental results is performed using the characteristics of the porous materials used in BJ experiments and reported in Table 1.

The porosity of the samples, not given in the reference paper is estimated from the classical Carman–Kozeny equation [60]. The estimation of the porosity for foametal samples with a fibrous structure is confirmed by a relation for fibrous lattices [61], which gives $\varepsilon_{\mathrm{f}} = 0.74$. Obviously, these estimations are better suited

Table 1
Geometrical characteristics of the porous specimens used in BJ experiments

Porous specimen	Permeability K [m^2]	Pore size d_{p} [m]	Porosity ε_{f}
Foametal	7.1×10^{-9}	–	0.78
Foametal A	9.7×10^{-9}	4.06×10^{-4}	0.78
Foametal B	3.94×10^{-8}	8.64×10^{-4}	0.78
Foametal C	8.2×10^{-8}	1.14×10^{-3}	0.79
Aloxite 1	6.45×10^{-10}	3.30×10^{-4}	0.58
Aloxite 2	1.6×10^{-9}	6.86×10^{-4}	0.52

The pore size of foametal is not given (first line), but its porosity is assumed to be the same as A, B, C, due to the similarities with these samples.

Table 2
Comparison with the analytical solution for foametal, $K = 7.1 \times 10^{-9}$ m^2, $\varepsilon_f = 0.78$

Darcy number	Analytical solution [19]		Numerical solution (This work)	
Da	$v(0)$	δ	$v(0)$	δ
1.02×10^{-1}	189.6	−1.610	189.5	−1.595
4.50×10^{-2}	116.8	−1.218	116.73	−1.218
1.97×10^{-2}	72.70	−0.888	72.60	−0.888
1.10×10^{-2}	52.46	−0.704	52.38	−0.704
9.50×10^{-3}	48.38	−0.660	48.31	−0.663
6.70×10^{-3}	39.96	−0.575	39.88	−0.575
5.00×10^{-3}	34.10	−0.510	34.02	−0.509
2.68×10^{-3}	24.43	−0.390	24.30	−0.392

than the arbitrary choice ($\varepsilon_f = 0.4$) used in previous studies [42].

2.1. Comparison with analytical solutions

The comparison between the numerical and analytical results is presented in Table 2 which reports, for different Darcy numbers, the slip velocity $u(0)$ and the dimensionless thickness of the porous boundary layer [19]

$$\delta = \sqrt{Da}\ln\left(\left[\frac{50(\sigma^2-2)}{1+\sigma\alpha}\right]^{\alpha}\right) \tag{14}$$

The agreement is also illustrated by the velocity profiles displayed in Fig. 2. The reduced viscosity expression retained in the calculations, $\mu_{eff}/\mu_f = \varepsilon_f^{-1}$, is obtained from the Darcy–Brinkman model derivation using volume averaging [62,63]. Others expressions for the reduced viscosity have also been used and it is verified that the agreement with the analytical results does not depend on the particular expression of the reduced viscosity. As opposed to Kuznetsov [54] and according to Angot [64] our results confirm that the single-domain approach implicitly imposes shear stress continuity whatever the reduced viscosity. This is clearly illustrated in Fig. 3 where the velocity profile at the interface is enlarged: the discontinuity of the velocity derivative is more visible for smaller porosity, e.g. $\varepsilon_f = 0.4$, and multiplying the value on both sides by the corresponding viscosity confirms that the single-domain approach implicitly imposes shear stress continuity.

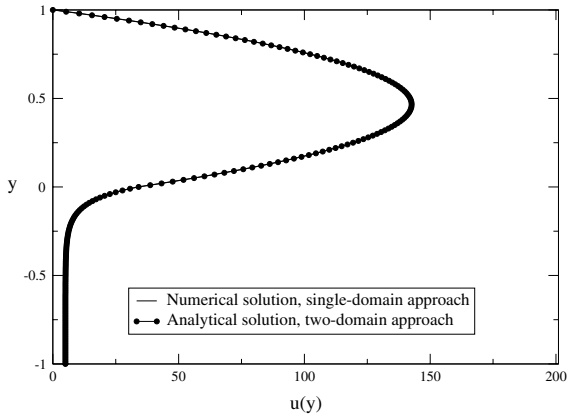

Fig. 2. Velocity profile: comparison between numerical (single-domain) and analytical (two-domain) solutions. Foametal material, $Da = 5 \times 10^{-3}$, $\varepsilon_f = 0.78$.

2.2. Comparison with experiments

The comparison with BJ experiments for the same foametal sample is shown in Fig. 4 in terms of the fractional increase in mass flow rate Φ due to the presence of the porous wall [8]

$$\Phi = \frac{Q_p - Q_i}{Q_i} = \frac{3(\sigma + 2\sqrt{\alpha})}{\sigma(1+\sigma\sqrt{\alpha})} \tag{15}$$

where Q_p is the mass flow rate within the fluid region for a given porous layer, while Q_i represents the flow rate for an impermeable porous wall ($Da \to 0$). The numerical simulation using the viscosity law $\mu_{eff}/\mu_f = \varepsilon_f^{-1}$ shows good agreement with the analytical solution for $\alpha = 1.2$

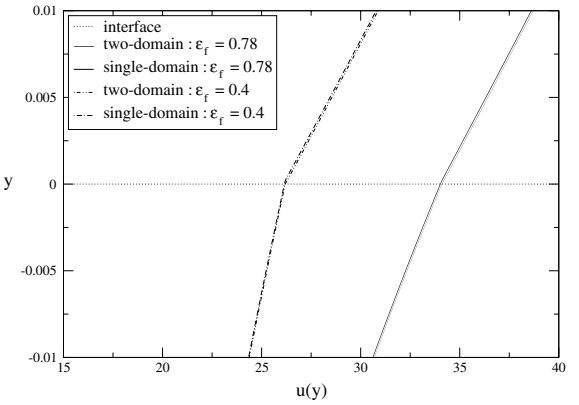

Fig. 3. Velocity profile: zoom at the fluid/porous interface.

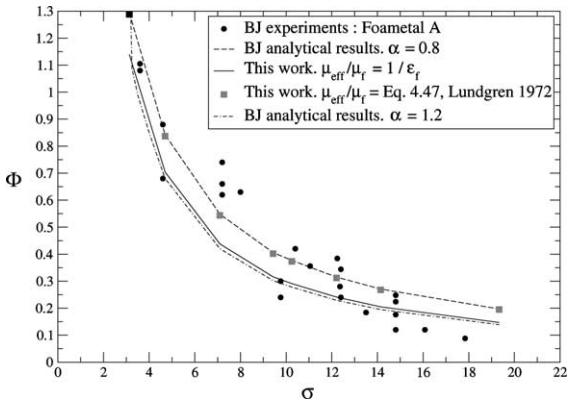

Fig. 4. Fractional excess flow rate Φ versus σ for the first Foametal. $K = 7.1 \times 10^{-9}$ m^2, $\varepsilon_f = 0.78$.

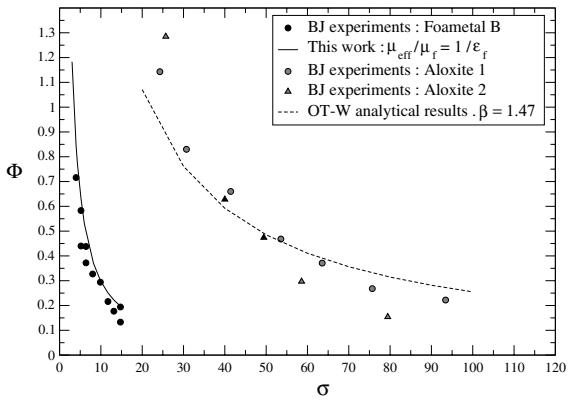

Fig. 5. Fractional excess flow rate Φ versus σ for Aloxite 1 and 2. Comparison between homogeneous single-domain approach, analytical solution (jump condition, OT-W) and BJ experiments.

while the scattered experimental data points are better fitted for $\alpha = 0.8$ [8]. Unfortunately, $\alpha < 1$ leads to a non-physical value of the porosity for this viscosity law. Other viscosity-porosity relations may be used in the numerical model, and the square symbols in Fig. 4 show that the non-monotonic relation derived by Lundgren (Eq. (4.47) of [21]) gives an excellent agreement with the analytical solution for $\alpha = 0.8$.

The experimental data obtained for the different foametal samples could be similarly adjusted using different α-values but this is not discriminatory because all the foametal structures are homogeneous and have the same porosity. Actually, according to Table 1 it is clear that α depends on the structural characteristics of the porous medium at the interface. The dependence of the reduced viscosity on the pore size had already been pointed out by [8] and later by Martys et al. [35], but in both cases no explicit function was given. Some expressions for the permeability dependence were also provided for dilute porous suspensions or polymers (see the references given by Vigne-Adler et al. [45]) but general relations involving all the complexity of the porous structures are still to be found. As a conclusion, these results show that the choice of the reduced viscosity has a direct consequence on the *quantitative* description of momentum transport in the interfacial region.

In the second step, numerical calculations concerning granular aloxite specimens have been compared to experiments (Fig. 5): the numerical results do not fit at all the experiments. Whatever the effective viscosity variations, this discrepancy remains: this is consistent with the fact that the Brinkman term hardly influences the momentum transport in porous structures for $\varepsilon_f = 0.52$–0.58. Thus, such a difference has to be the consequence of the structure of the aloxite material which is shown to have a very irregular pore distribution close to the interface [8] leading to a much higher permeability in the porous boundary layer. For these structures, experimental results can be well fitted by the analytical solution by adjusting the slip coefficient α or the stress jump parameter β ($\beta = 1.47$ in Fig. 5) since these parameters implicitly account for the geometrical structure and the actual location of the interface. This is obviously not included in the present single-domain model where so far the porous layer has been assumed to be homogeneous. In order to overcome this limitation, a more general description is proposed in Section 3, introducing a non-homogeneous porous layer at the fluid/porous interface.

3. Non-homogeneous analysis

Since the structure of the interface is the origin of the discrepancies observed in Section 2, it may be useful to recall that an interface is an ideal representation of a region with *continuous spatial changes of the macroscopic properties* (porosity, permeability, effective viscosity) and that the knowledge of these "evolving heterogeneities" is necessary for an accurate description of transport phenomena near the interface. Indeed, for steep spatial variations of the geometry between the fluid and porous regions, a jump boundary condition (4) may be used while for smoother changes an alternative model consists in explicitly accounting for these spatial variations by introducing a non-homogeneous porous layer between the fluid and the homogeneous "bulk" porous medium, as shown in Fig. 6. This is the configuration considered in this section. In a first step, we show how the stress jump coefficient β is explicitly related to the geometrical characteristics of the non-homogeneous layer. Then, numerical solutions for the velocity field and the flow rate are compared to the experimental re-

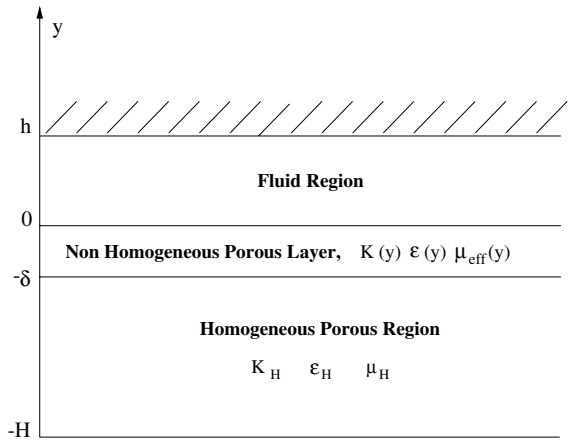

Fig. 6. Fluid/porous channel with non-homogeneous interfacial layer.

sults and to the analytical solution derived using the stress jump condition and quantitative values for β are obtained.

3.1. Stress jump coefficient

We consider the fluid/porous channel represented in Fig. 6. In the non-homogeneous zone of the porous layer ($-\delta \leqslant y \leqslant 0$), the macroscopic properties continuously vary from the bulk values (noted with subscript H) to the fluid values. Therefore, the one-dimensional momentum transport equation in the porous part of the channel takes the form

$$\frac{\partial}{\partial y}\left(\eta(y)\frac{\partial U}{\partial y}\right) = \left(\frac{U}{K(y)} - \frac{U(-H)}{K_{\mathrm{H}}}\right) \tag{16}$$

where $\eta(y) = \mu_{\mathrm{eff}}(y)/\mu_{\mathrm{f}}$ and $K(y)$ are the spatial variations of the reduced viscosity and permeability, respectively. In Eq. (16), the pressure gradient has been expressed using Darcy's law in the homogeneous porous medium

$$\frac{\partial P}{\partial x} = -\mu_{\mathrm{f}}\frac{U(-H)}{K_{\mathrm{H}}} \tag{17}$$

Integrating (16) over the non-homogeneous layer thickness (between $-\delta$ and 0), yields the jump shear stress

$$\left.\frac{\partial u}{\partial y}\right|_{y=0} - \eta_{\mathrm{H}}\left.\frac{\partial U}{\partial y}\right|_{y=-\delta} = \int_{-\delta}^{0}\left(\frac{U}{K(y)} - \frac{U(-H)}{K_{\mathrm{H}}}\right)\mathrm{d}y \tag{18}$$

If we compare Eq. (18) to (4), it appears that the meaning of β is related to the spatial variation of the permeability and velocity field. Since the porous layer is homogeneous for $-H < y < -\delta$, Eq. (16) in this latter region takes the form

$$\eta_{\mathrm{H}}\frac{\partial^2 U}{\partial y^2} = \left(\frac{U}{K_{\mathrm{H}}} - \frac{U(-H)}{K_{\mathrm{H}}}\right) \tag{19}$$

whose solution for $-H < y < -\delta$ is given by

$$U(y) = U(-H) + (U(-\delta) - U(-H))\exp\left(\frac{y}{\sqrt{\eta_{\mathrm{H}}K_{\mathrm{H}}}}\right) \tag{20}$$

Hence, the shear stress at $y = -\delta$ is

$$\left.\frac{\partial U}{\partial y}\right|_{y=-\delta} = \frac{1}{\sqrt{\eta_{\mathrm{H}}K_{\mathrm{H}}}}(U(-\delta) - U(-H)) \tag{21}$$

and therefore Eq. (18) becomes

$$\left.\frac{\partial u}{\partial y}\right|_{y=0} = \underbrace{\sqrt{\frac{\eta_{\mathrm{H}}}{K_{\mathrm{H}}}}(U(-\delta) - U(-H))}_{\text{Brinkman boundary layer}} + \underbrace{\int_{-\delta}^{0}\left(\frac{U}{K(y)} - \frac{U(-H)}{K_{\mathrm{H}}}\right)\mathrm{d}y}_{\text{Non-homogeneous layer}} \tag{22}$$

where two contributions are identified. The first term of the right-hand side in (22) represents the Brinkman boundary layer in the homogeneous porous region while the second term is the contribution of the non-homogeneous layer. Integrating (16) between y and 0 leads to

$$\frac{\partial U}{\partial y} = \frac{1}{\eta(y)}\left[\left.\frac{\partial u}{\partial y}\right|_{y=0} - \int_{y}^{0}\left(\frac{U}{K(z)} - \frac{U(-H)}{K_{\mathrm{H}}}\right)\mathrm{d}z\right] \tag{23}$$

and a new integration of (23) between $-\delta$ and 0 provides $U(-\delta)$ under the form

$$U(-\delta) = u(0) - l(0)\left.\frac{\partial u}{\partial y}\right|_{y=0} + \int_{-\delta}^{0} l(y)\left(\frac{U}{K(y)} - \frac{U(-H)}{K_{\mathrm{H}}}\right)\mathrm{d}y \tag{24}$$

where $l(y)$ is defined by

$$l(y) = \int_{-\delta}^{y}\frac{\mathrm{d}z}{\eta(z)} \tag{25}$$

Finally, using (24) in (22), we obtain the shear stress constraint at the fluid/porous interface

$$\left.\frac{\partial u}{\partial y}\right|_{y=0} = \frac{1}{1+\mathscr{L}(0)}\sqrt{\frac{\eta_{\mathrm{H}}}{K_{\mathrm{H}}}}(u(0) - U(-H)) + \int_{-\delta}^{0}\frac{1+\mathscr{L}(y)}{1+\mathscr{L}(0)}\left(\frac{U}{K(y)} - \frac{U(-H)}{K_{\mathrm{H}}}\right)\mathrm{d}y \tag{26}$$

where

$$\mathscr{L}(y) = \sqrt{\eta_{\mathrm{H}}/K_{\mathrm{H}}}\,l(y) \tag{27}$$

Identifying Eq. (26) with the boundary condition (5), the stress-jump coefficient is explicitly determined

$$\beta = \frac{\sqrt{K_H}}{u(0)}\left\{\frac{\mathscr{L}(0)}{1+\mathscr{L}(0)}\sqrt{\frac{K_H}{\eta_H}}(u(0)-U(-H)) - \int_{-\delta}^{0}\frac{1+\mathscr{L}(y)}{1+\mathscr{L}(0)}\left(\frac{U}{K(y)}-\frac{U(-H)}{K_H}\right)dy\right\} \quad (28)$$

Eq. (28) clearly shows that *the stress-jump coefficient β is explicitly related to the continuous spatial variations of the porous structure near the interface*. We can also note that, according to Section 2, Eq. (26) also satisfies the shear stress continuity condition (9) for an homogeneous porous medium ($\delta = 0$) since

$$\lim_{\delta\to 0}\mathscr{L}(0) = 0 \Rightarrow \lim_{\delta\to 0}\beta = 0 \quad (29)$$

Actually, the geometry-dependence of β has already been emphasized by Ochoa-Tapia and Whitaker [41] using a volume averaging procedure. In their analysis, β is found to be a very complex function of the closure variables for which even the derivation of the local closure problems still remains a challenge. Moreover, if these problems would be known, their numerical resolution would suppose a detailed knowledge of the *microstructure* of the fluid-porous inter-region. On the contrary, as shown below, relation (28) is found to be much more general since β can be directly computed from the numerical solution of the non-homogeneous single-domain approach and finally compared to the empirical values used in the analytical solution to fit the experiments. In the present approach, the main unknowns remain the dimensionless thickness δ of the non-homogeneous layer and the type of spatial variations of the averaged properties. This issue will be discussed in the next section.

3.2. Numerical calculations and comparison with experiments

Eq. (16) is solved numerically in the whole channel (Fig. 6) using the single-domain approach. The numerical strategy is the following: for a given spatial evolution of the averaged properties of the non-homogeneous porous layer, its thickness δ is adjusted to fit the interfacial velocity and the flow rate measured in the BJ experiments. Then, the numerical integration of (28) yields the associated stress jump coefficient β, which is compared to the values estimated from the analytical solution. Due to the lack of information concerning the spatial change of the average properties, the spatial variation of the porosity is first assumed to be linear. The permeability is then obtained by the Carman–Kozeny relation and, according to Ochoa-Tapia and Whitaker [42], the non-homogeneous reduced viscosity is $\eta(y) = \varepsilon_f^{-1}$.

Numerical results for Aloxite 1 and 2 represented in Fig. 7 show a very good agreement with the experiments and analytical results. The significant improvement brought by the introduction of a non-homogeneous porous layer is clear when comparing to the results in Fig. 5. The corresponding variation of the non-homogeneous porous layer thickness with σ is plotted in Fig. 8 where the total boundary layer thickness at the interface is also displayed

$$\delta_T = \delta + \delta_B, \quad (30)$$

where according to Eq. (22), δ_B stands for the Brinkman boundary layer in the homogeneous porous region. First, as expected, δ decreases when the Darcy number decreases. This is also true for δ_T, and it is easy to verify that $\delta_B \to 0$ with decreasing Darcy numbers, since the Brinkman term becomes negligible at low permeabilities

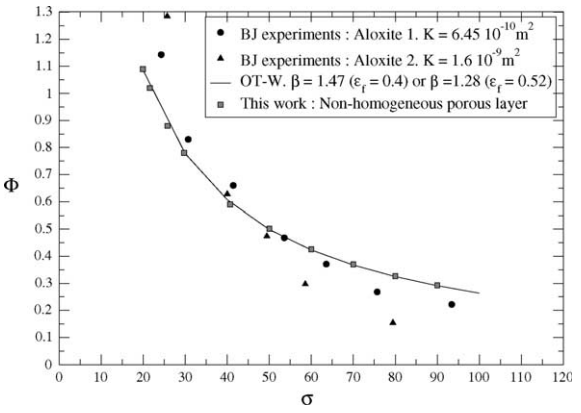

Fig. 7. Fractional excess flow rate Φ versus σ for Aloxite 1 and 2. Comparison between non-homogeneous interfacial layer (single-domain approach), analytical solution (jump condition, OT-W) and BJ experiments. Note that in this reference, $\varepsilon_f = 0.4$ and $\beta = 1.47$: since the present calculations are performed using $\varepsilon_f = 0.52$, the corresponding value of the stress jump coefficient for analytical solution is $\beta = 1.28$.

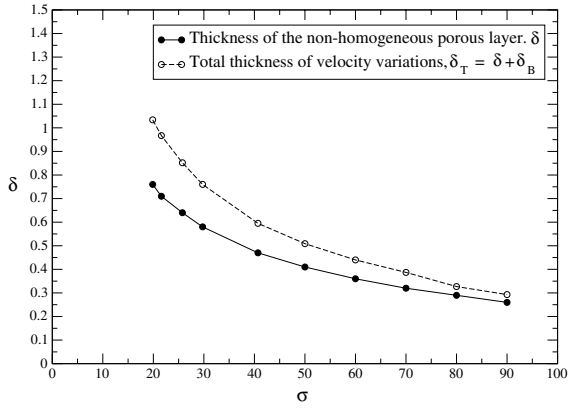

Fig. 8. Thickness of the non-homogeneous porous layer.

Table 3
Evolution of δ_T/d_p^* *versus* the Darcy number

Da	d_p^*	δ_T	δ_T/d_p^*
1.02×10^{-2}	1.73	1.73	1
4.45×10^{-3}	1.144	1.28	1.12
2.53×10^{-3}	0.863	1.034	1.2
2.14×10^{-3}	0.794	0.967	1.22
1.51×10^{-3}	0.666	0.852	1.28
1.13×10^{-3}	0.576	0.760	1.32
6.04×10^{-4}	0.42	0.595	1.41
4×10^{-4}	0.343	0.509	1.483
2.78×10^{-4}	0.284	0.44	1.55
1.23×10^{-4}	0.191	0.311	1.63

and the viscous layer vanishes. In Table 3 we report the variation of δ_T with the dimensionless average pore size $d_p^* = d_p/h$ (note that in the BJ experiments the permeability of the aloxite is a constant and that the Darcy number is varied through the height h of the fluid channel). These results show that δ_T/d_p^* hardly increases with the Darcy number and according to theoretical studies [11,38] we may write

$$\frac{\delta_T}{d_p^*} \sim O(1) \tag{31}$$

Therefore for a given porous material

$$\delta_T \sim A\sqrt{Da} \tag{32}$$

where $A = d_p/\sqrt{K}$ is a constant which depends on the porous specimen (according to BJ data, $A = 4$ for the three foametal structures, $A = 13$ for Aloxite 1 and $A = 17$ for Aloxite 2). If we turn our attention to the velocity profiles displayed in Fig. 9, a significant difference between analytical and numerical results is observed within the transition layer. This discrepancy is not surprising since the two-domain analytical solution assumes that the porous layer is homogeneous, the geometry of the interface being implicitly included in the stress jump coefficient β while spatial variations are explicitly included in the momentum transport equation (16).

This analysis shows that the procedure for estimating δ may be applied to the aloxite experiments at different Darcy numbers. Then the stress jump coefficient β can be identified from Eq. (28): Fig. 10 displays the values of β obtained for the σ-range covered by BJ experiments. This *remarkable agreement* with the adjusted value arising from the analytical solution proves that the non-homogeneous model is able to quantify the effect of the morphology of the fluid-porous interface. This morphology is different for each sample, and it is even possible to make a distinction between the two aloxite samples using this analysis: the average β value is thus found to be of 1.23 for Aloxite 1 and 1.30 for Aloxite 2. Thus, it seems that this procedure allows to detect rather small differences between similar samples.

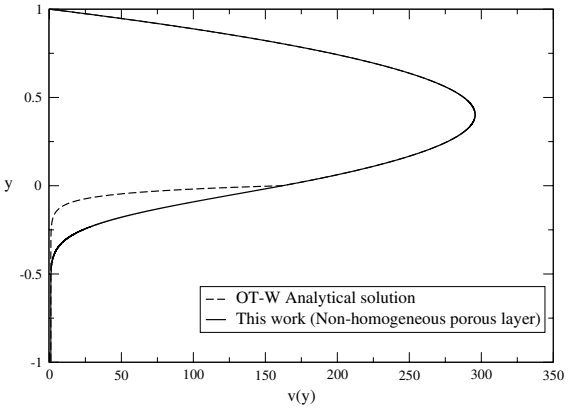

Fig. 9. Comparison of the velocity profiles. Porosity: linear variation, $\varepsilon_H = 0.52$; permeability: Carman–Kozeny, $\sigma = 40.7$; $\eta(y) = 1/\varepsilon_f(y)$.

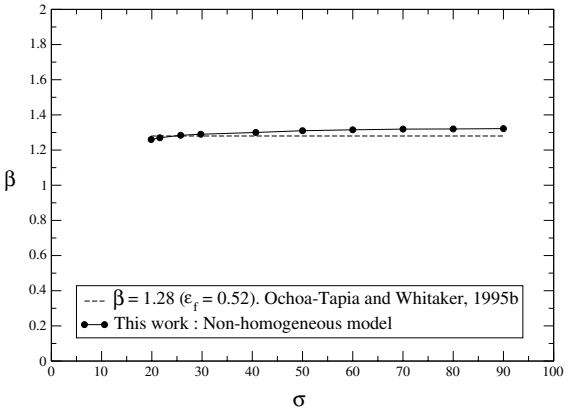

Fig. 10. Stress jump coefficient.

In order to generalize the above results, we now have to examine the influence of the variation law retained for the porosity and permeability in the non-homogeneous layer. Keeping first the Carman–Kozeny relation for the permeability, several spatial porosity variations have been used in the calculations (Fig. 11) and consequences on the ratio δ_T/d_p^* are presented in Table 4. It is shown that for all the porosity laws considered here, the ratio δ_T/d_p^* remains on the order of one. More precisely, the dependence on Darcy number is less sensitive for sharper porosity profiles (a factor 1.6 for a linear variation against 1.38 for the error function). A comparison of the velocity profiles for $Da = 6.04\times10^{-4}$ (Fig. 12) shows a relatively small influence of the spatial porosity variations on the velocity. This is related to the very thin non-homogeneous porous thickness and the same observation is done for the spatial permeability variations, whose influence is limited to a very few % on δ and velocity profiles.

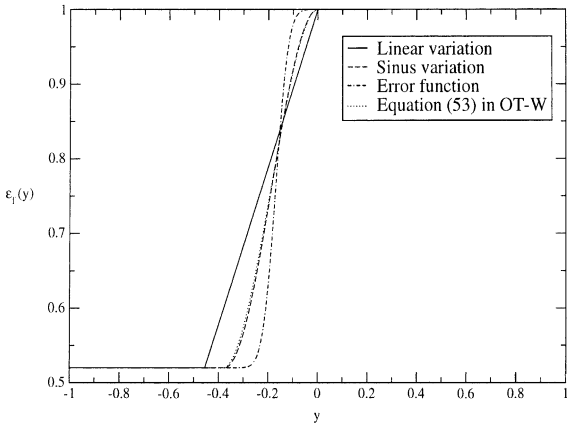

Fig. 11. Spatial porosity variations.

Table 4
δ_T/d_p^* for three spatial porosity functions

Da	δ_T/d_p^*		
	Porosity variations		
	Linear	Sinusoidal	Error function
1.02×10^{-2}	1	0.92	0.92
2.53×10^{-3}	1.2	1.06	0.985
1.13×10^{-3}	1.32	1.145	1.042
6.04×10^{-4}	1.41	1.207	1.1
2.78×10^{-4}	1.55	1.296	1.16
1.23×10^{-4}	1.63	1.33	1.194

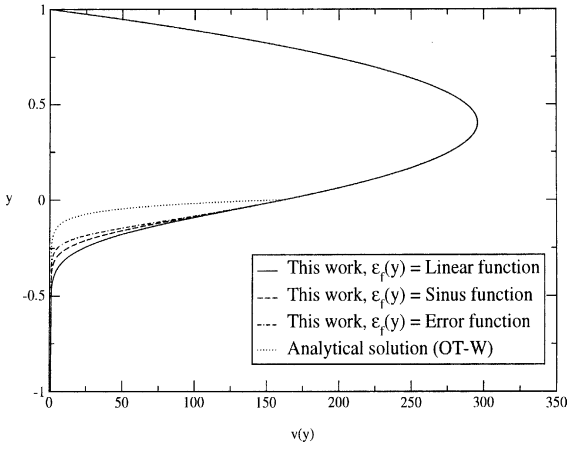

Fig. 12. Influence of the spatial porosity variations on the velocity profile.

As a conclusion of the comparison between the homogeneous and the non-homogeneous models commented in Fig. 9, we can assess that the stress jump boundary condition resulting from the use of an homogeneous formulation is able to give an accurate representation of the momentum transport only in the fluid channel, or for a configuration with rapid spatial changes of the average properties near the interface, e.g. for extremely thin non-homogeneous layers that would be very difficult to discretize numerically. The drawbacks of the approach lie in the fact that β remains an adjustable parameter and that the description of the flow in the porous layer is only an approximation. On the contrary, the non-homogeneous single-domain description is very attractive by its ability to provide a complete description of the flow in the whole channel, without the need of adjustable parameters. It may also be applied to give an accurate estimation of the value of β to be used in an homogeneous model, simply based on the knowledge of the dimensionless pore size.

4. Conclusion

After reviewing the approaches proposed by various authors for modeling momentum balance at the interface between a liquid and a porous substrate, a new interfacial model has been derived. First, we have shown that the single-domain representation and the different formulation of the two-domain models are equivalent when the porous layer is *homogeneous* ($\beta = 0$). Then, when $\beta \neq 0$, the analysis of the interfacial region, using a non-homogeneous transition layer presenting continuous variations of the effective properties, has permitted to provide an explicit expression and a physical content to the adjustable parameter accounting for jump boundary condition at the interface which results from the stress variations across the non-homogeneous layer. A very good agreement has been found between our numerical results based on the single-domain approach and the existing *ad hoc* estimates in the literature. This analysis allowed us to clarify why the various models usually considered in the literature (single- or two-domains approaches) are equally useful depending on the particular morphology of the interface.

Finally, we conclude that our analysis constitutes an "intermediate" step towards the exact determination of β, which would imply to write a general closure problem at the fluid/porous interface, which still remains a challenge. This discussion might actually have a broader scope than the particular configuration under study in this paper, and such an analysis could be relevant to other widely studied situations, such as for example, the onset of erosion instabilities in a fluid flow along a granular layer.

Acknowledgements

The authors wish to gratefully thank M.G. Homsy and E.J. Hinch for fruitful discussions and advice.

References

[1] M. Kaviany, Principles of Heat Transfer in Porous Media, second ed., Springer-Verlag, New York, 1995.
[2] D.A. Nield, A. Bejan, Convection in Porous Media, Springer-Verlag, New York, 1998.
[3] S.I. Gheorghiţă, Com. Acad. Repub. Pop. Rom. 5 (1955) 661–662.
[4] D.D. Joseph, L.N. Tao, Z. Angew. Math. Mech. 44 (1964) 361–364.
[5] S.I. Gheorghiţă, Z. Angew. Math. Mech. 46 (1966) 135–139.
[6] J.H. Masliyah, M. Polikar, Can. J. Chem. Eng. 5 (1980) 299–302.
[7] D.D. Joseph, L.N. Tao, J. Appl. Mech. 33 (1966) 753–760.
[8] G.S. Beavers, D.D. Joseph, J. Fluid Mech. 30 (1967) 197–207.
[9] P.G. Saffman, Stud. Appl. Mech. L (1971) 93–101.
[10] S. Saleh, J.F. Thovert, P.M. Adler, AIChE J. 39 (11) (1993) 1765–1776.
[11] R.E. Larson, J.J.L. Higdon, J. Fluid Mech. 166 (1986) 449–472.
[12] R.E. Larson, J.J.L. Higdon, J. Fluid Mech. 178 (1987) 119–136.
[13] G.S. Beavers, E.M. Sparrow, R.A. Magnuson, J. Basic Eng. 92 (1970) 843–848.
[14] G.I. Taylor, J. Fluid Mech. 49 (1971) 319–326.
[15] S. Richardson, J. Fluid Mech. 49 (1971) 327–336.
[16] G.S. Beavers, E.M. Sparrow, B.A. Masha, AIGhe J. 20 (3) (1974) 596–597.
[17] W. Jäger, A. Mikelić, SIAM J. Appl. Math. 60 (4) (2000) 1111–1127.
[18] H.C. Brinkman, Appl. Sci. Res. A 1 (1947) 27–34.
[19] G. Neale, W. Nader, Can. J. Chem. Eng. 52 (1974) 475–478.
[20] C.K.W. Tam, J. Fluid Mech. 38 (1969) 537–546.
[21] T.S. Lundgren, J. Fluid Mech. 51 (1972) 273–299.
[22] T. Levy, CR Acad. Sci. 292 (Serie II) (1981) 872–874.
[23] D.A. Nield, J. Fluid Mech. 128 (1983) 37–46.
[24] S. Kim, W.B. Russel, J. Fluid Mech. 154 (1985) 269–286.
[25] J. Rubinstein, J. Fluid Mech. 170 (1986) 379–383.
[26] L. Durlofsky, J.F. Brady, Phys. Fluids 30 (11) (1987) 3329–3341.
[27] K. Vafai, S.J. Kim, Int. J. Heat Fluid Flow 11 (3) (1990) 254–256.
[28] D.A. Nield, Int. J. Heat Fluid Flow 12 (3) (1991) 269–272.
[29] K. Vafai, S.J. Kim, Int. J. Heat Fluid Flow 16 (1995) 11–15.
[30] K.F. Freed, M. Muthukumar, J. Chem. Phys. 68 (5) (1978) 2088–2096.
[31] P.M. Adler, Rheol. Acta 17 (1978) 288–295.
[32] P.M. Adler, P.M. Mills, J. Rheol. 23 (1) (1979) 25–37.
[33] J. Koplik, H. Levine, A. Zee, Phys. Fluids 26 (10) (1983) 2864–2870.
[34] J.A. Kolodziej, Acta Mech. 75 (1988) 241–254.
[35] N. Martys, D.P. Bentz, E.J. Garboczi, Phys. Fluids 6 (4) (1994) 1434–1439.
[36] R.C. Givler, S.A. Altobelli, J. Fluid Mech. 258 (1994) 355–370.
[37] A. Einstein, Ann. Phys. 19 (4) (1906) 289–306, trans. in 1956, Theory of the Brownian movement, Dover.
[38] M. Sahraoui, M. Kaviany, Int. J. Heat Mass Transfer 35 (4) (1992) 927–943.
[39] V.M. Starov, V.G. Zhdanov, Colloids Surf. A: Physicochem. Eng. Aspects 192 (2001) 363–375.
[40] J. Bear, Y. Bachmat, Introduction to Modeling of Transport Phenomena in Porous Media, Kluwer Academic, 1990.
[41] J.A. Ochoa-Tapia, S. Whitaker, Int. J. Heat Mass Transfer 38 (1995) 2635–2646.
[42] J.A. Ochoa-Tapia, S. Whitaker, Int. J. Heat Mass Transfer 38 (1995) 2647–2655.
[43] A.V. Kuznetsov, Int. C. Heat Mass Transfer 24 (3) (1997) 401–410.
[44] A.V. Kuznetsov, Int. J. Heat Mass Transfer 41 (16) (1998) 2556–2560.
[45] M. Vignes-Adler, P.M. Adler, P. Gougat, PCH Physicochem. Hydrodynam. 8 (4) (1987) 401–422.
[46] A.S. Sangani, S. Behl, Phys. Fluids A 1 (1) (1988) 21–37.
[47] D.F. James, A.M.J. Davis, J. Fluid Mech. 426 (2001) 47–72.
[48] E. Arquis, J. Caltagirone, CR Acad. Sci. 299-II (1984) 1–4.
[49] C. Beckermann, S. Ramadhyani, R. Viskanta, ASME J. Heat Transfer 109 (1987) 363–370.
[50] C. Beckermann, R. Viskanta, S. Ramadhyani, J. Fluid Mech. 186 (1988) 257–284.
[51] S. Turki, G. Lauriat, An examination of two numerical procedures for natural convection in composites enclosures, in: Numerical Heat Transfer Proceedings of AIAA–ASME Thermophysics and Heat Transfer Conference, HTD, vol. 130, 1990, pp. 107–113.
[52] P. LeBreton, J.P. Caltagirone, E. Arquis, ASME J. Heat Transfer 113 (1991) 892–898.
[53] J. Ettefagh, K. Vafai, S.J. Kim, ASME J. of Heat Transfer 113 (1991) 747–756.
[54] A.V. Kuznetsov, Ming-Xiong, Hybrid Meth. Eng. 1 (1999) 249–264.
[55] J. Mercier, C. Weisman, M. Firdaous, P.L. Quéré, ASME J. Heat Transfer 124 (2002) 130–143.
[56] D. Gobin, D. Goyeau, J. Songbe, ASME J. Heat Transfer 120 (1998) 234–242.
[57] B. Goyeau, D. Gobin, Int. Comm. Heat Mass Transfer 26 (8) (1999) 1115–1126.
[58] M. Song, R. Viskanta, Int.J. Heat Mass Transfer 37 (16) (1994) 2425–2438.
[59] S.V. Patankar, Numerical Heat Transfer and Fluid Flow, McGraw-Hill, New York, NY, 1980.
[60] P. Carman, Trans. Inst. Chem. Eng. London 15 (1937) 150–166.
[61] G.W. Jackson, D.F. James, Can. J. Chem. Eng. 64 (1986) 364–374.
[62] S. Whitaker, Transport Porous Med. 1 (1986) 3–35.
[63] M. Quintard, S. Whitaker, Transport Porous Med. 15 (1994) 31–49.
[64] P. Angot, Math. Meth. Appl. Sci. 22 (16) (1999) 1395–1412.